Pergamon

PII: S0967-0637(96)00097-6

Deep-Sea Research I, Vol. 43, No. 4, pp. 555–578, 1996

0967-0637/96 $15.00 + 0.00

Eddy formation behind the tropical island of Aldabra

KAREN J. HEYWOOD,* DAVID P. STEVENS† and GRANT R. BIGG*

(*Received* 1 *March* 1995; *accepted* 23 *August* 1995)

Abstract—Oceanic eddy formation behind the tropical island of Aldabra is examined with a one-layer reduced gravity model. Thresholds for flow separation, eddy formation, eddy shedding, and wake instabilities are determined and compared with theory, observations and results of laboratory experiments for both rotating and non-rotating flows. It is shown that non-rotating fluid theory and the Reynolds number are appropriate for describing the occurrence of eddy shedding. For islands at higher latitudes, thresholds move nearer those found in rotating laboratory experiments. Strouhal numbers calculated from the model results agree with those predicted theoretically, confirming that the frequency of eddy shedding does not increase indefinitely with Reynolds number. Both the model results and data from the CZCS archive suggest that eddy shedding and the associated enhanced biological activity (and thus CO_2 uptake) are common phenomena for Aldabra and, by implication, other oceanic islands. Copyright © 1996 Elsevier Science Ltd

1. INTRODUCTION

It is well known that fluid flow past topography may lead to eddies, either trapped or spun off into a wake, for example, vortex streets shown in cloud patterns in the lee of mountains (Gjevik, 1980) and in currents around islands (Hogg, 1980). Laboratory experiments (Boyer and Davies, 1982) have shown that on a rotating Earth cyclonic vortices are stronger than anticyclonic ones; this is also seen in cloud streets (Scorer, 1986). These eddies may affect the momentum and kinetic energy of the mean flow. There is also a significant influence on the biological productivity (the "island mass effect", see for example Gilmartin and Revelante (1974)).

A trapped eddy was observed in the lee of the oceanic island of Aldabra (47°30′E, 9°45′S—see Fig. 1), situated in the South Equatorial Current (SEC) of the Indian Ocean, during a cruise in 1987 (Heywood *et al.*, 1990). The island is an isolated steep sided atoll (inset of Fig. 1). Therefore, the influence of bottom drag is not important in this "dynamically deep" situation, as discussed by Tomczak (1988). The integrated chlorophyll content of the upper ocean was found to increase markedly in the eddy formed behind Aldabra. These isolated patches of higher primary production will be advected downstream with a shed eddy and may help to explain the patchiness of zooplankton distributions (Heywood *et al.*, 1991).

In this paper we consider a numerical model of the flow around Aldabra. This enables us to determine the range of conditions under which eddies are trapped or shed. Using knowledge of the climatological currents in this area of the Indian Ocean, we are able to see for which months of a typical year eddy shedding is significant.

*School of Environmental Sciences, University of East Anglia, Norwich NR4 7TJ, U.K.
†School of Mathematics, University of East Anglia, Norwich NR4 7TJ, U.K.

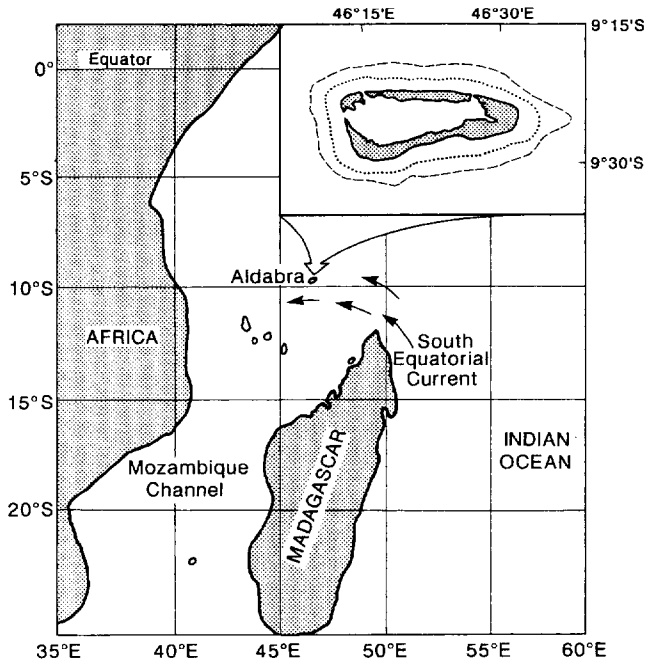

Fig. 1. The location of the island of Aldabra in the Indian Ocean. The inset illustrates the bathymetry. The dotted contour indicates the 1000 m isobath and the dashed line indicates the 2000 m isobath.

2. OBSERVATIONS

Observations of the current flow around Aldabra were taken during April to July 1987 from the R.R.S. *Charles Darwin* with the shipborne acoustic Doppler current profiler (ADCP) (Heywood *et al.*, 1990). The ADCP yields currents relative to the ship, so accurate navigation is necessary to calculate currents relative to the ground. However good GPS fixes occurred during the cruise for less than 2 h per day; therefore, it was not possible to calculate accurate absolute currents while the ship was moving.

Heywood *et al.* (1990) showed currents while the ship was on station during CTD casts, so errors due to infrequent transit satellite fixes were small. With an incident current of about 0.6 m s^{-1} from the east-southeast, an eddy was observed as a region of reduced sea surface temperature and increased sea surface salinity. This was associated with a doubling of the chlorophyll content of the water column. One would expect the currents to be circulating around this eddy cyclonically (clockwise in the southern hemisphere). The ADCP currents showed a speeding up as the water passed the island, and a confused region in the lee, but no clear eddy could be seen. This was probably because the survey took about 3 days to complete and the system would not have been in local steady state.

Some additional rapid surveys were undertaken with the ADCP alone, without stopping for CTD stations. In this way, a more synoptic picture could be obtained, since a similar area could be covered in about 1 day. Since the ship was steaming and turning, transit satellite fixes are not adequate to provide accurate navigation to calculate absolute currents from the ADCP. Instead, we show near-surface currents at 19 m relative to a reference level

of about 400 m. The pycnocline is situated at about 100 m, and we are assuming that most of the shear occurs there. Current meter data from moorings near Aldabra support the assumption of small currents at the depth of the reference level.

The first rapid survey (27–29 June) shows an incident farfield current from the south with a magnitude of about 0.2 m s^{-1} (Fig. 2(a)). At this time Aldabra presented its widest cross-section to the current. The current does not seem to be large enough to generate an eddy, but the water flowing round the western edge of Aldabra turns east in the lee. As was found by the laboratory experiments of Boyer and Davies (1982), the current is enhanced more on the left than the right (see for example Fig. 5(a) in that paper, which is applicable to the northern hemisphere). In their experiments the lee is a fairly stagnant area where no dye lines reached. In our survey, the currents on the right hand side are also weaker.

The second survey (4–6 July) took place during a period of incident current from the east (Fig. 2(b)), so Aldabra presented its smallest cross-section to the flow. The farfield flow is about 0.3 m s^{-1}. A small eddy (marked "A") is suggested by the ADCP currents to the southwest of Aldabra. As was noted by Heywood *et al.* (1990), the size of the eddy is about the same as the cross-sectional diameter presented by the island to the flow.

These observations, although not conclusive, suggest that eddies do occur in the wake of Aldabra under sufficiently strong flow. As discussed in Heywood *et al.* (1990), the SEC is usually stronger in this area, and a vortex street of eddies might be expected. The zonal wind, and the entire Indian Monsoon circulation system, was weaker than normal in 1987 (Anderson and Carrington, 1993). As will be shown, this may have been the reason for inconclusive evidence for eddy shedding during the cruise. In this paper we shall use a numerical model to study the creation of these eddies further.

The SEC varies relatively little in this region over the year (Cutler and Swallow, 1984), unlike the surface circulation north of the equator. Surface currents near Aldabra were extracted from the Cutler and Swallow (1984) atlas. A seasonal time series of the current speed climatology is illustrated in Fig. 3. The current displays a small seasonal cycle peaking between June and October, and exhibiting lowest values between December and April. 50% of the speeds are greater than 0.45 m s^{-1}. During June–October, 80% lie above this threshold. The mean direction is 270°; all except four of the 36 values lie within 240°–300°, and all these are in January or February when the currents are at their weakest. The mean speed during the year is 0.47 m s^{-1} with a standard deviation of 0.18 m s^{-1}.

3. BIOLOGICAL SIGNIFICANCE

To determine whether the enhancement of chlorophyll content around Aldabra is indeed significant on an annual timescale, we have extracted from the global archive all Coastal Zone Color Scanner (CZCS) images covering the Aldabra region. These are calibrated to chlorophyll (mg m^{-3}) and are of 4 km resolution. In all, 47 reasonably cloud-free images were studied, from 1979 to 1986. Each image was examined for evidence of enhanced chlorophyll around or downstream of Aldabra. Pixels immediately adjacent to the island may be contaminated, so these were ignored.

Of the 46 images in which Aldabra itself was cloudfree, seven had a significant enhancement of chlorophyll, and a further 14 showed a small effect (Table 1). These indicate the presence of a trapped eddy immediately behind the island. The greater chlorophyll values were always to the north, northwest or west. Typically chlorophyll was increased from 0.1 to 0.2 mg m^{-3}. Usually the enhancement was close to the island, but in

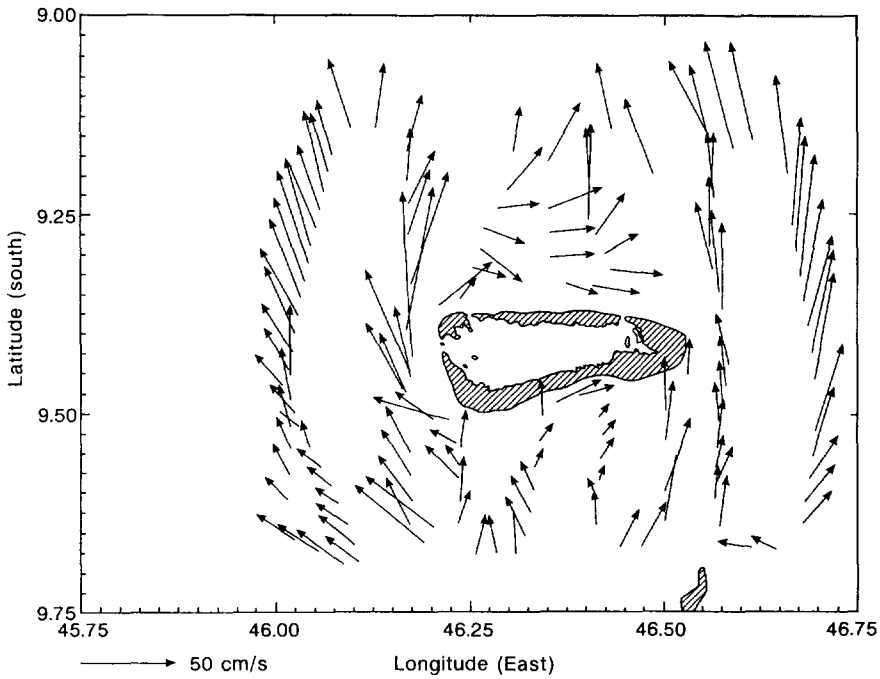

(a)

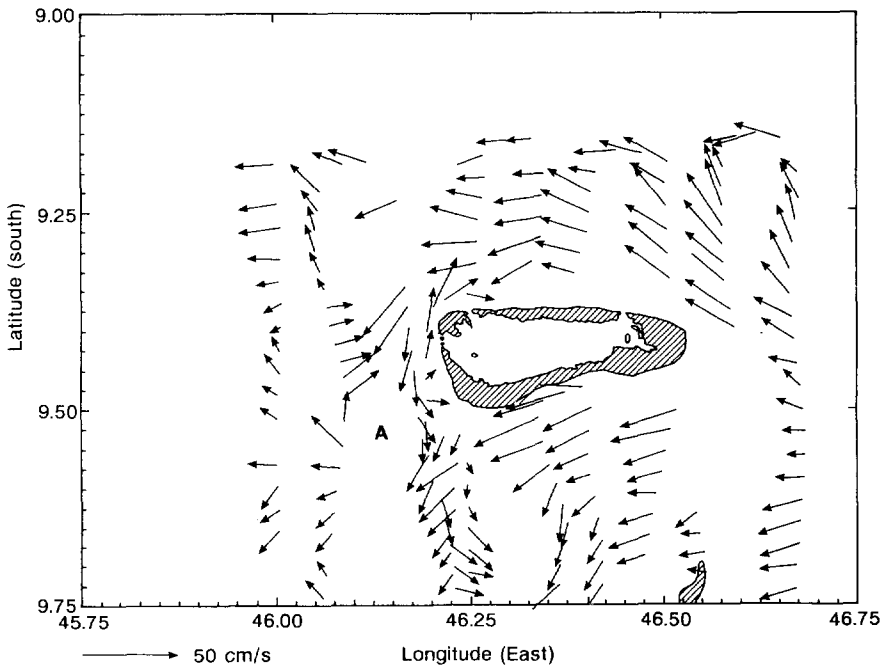

(b)

Fig. 2. Observations of the current at 19 m taken during R.R.S. *Charles Darwin* cruise 24 with shipborne acoustic Doppler current profiler (ADCP). Currents relative to a reference level of 400 m (a) first survey, 27–29 June 1987 and (b) second survey, 4–6 July 1987.

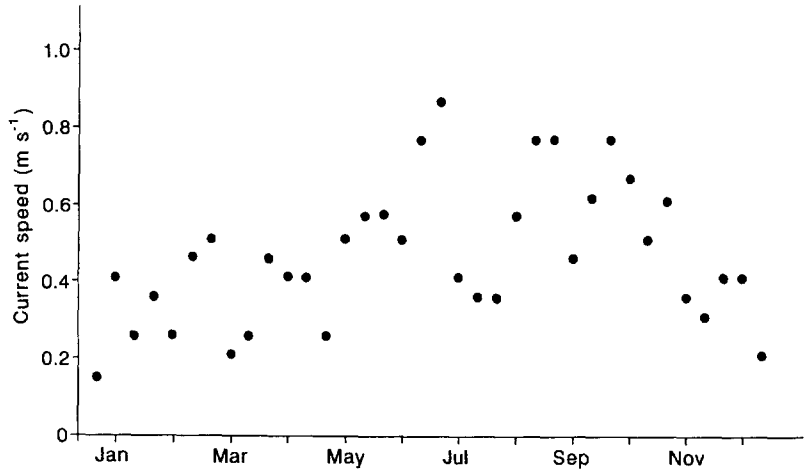

Fig. 3. A time series of the magnitude of surface currents [extracted from the Cutler and Swallow (1984) atlas] near Aldabra for a climatological year.

three cases there appeared to be an eddy of enhanced productivity just downstream. An example of increased chlorophyll to the north-west of Aldabra is given in Fig. 4.

Investigation of seasonal effects is complicated by the variable nature of cloud cover. In February, May, August, September and October, there were insufficient images to draw any significant conclusion. The clearest months are April, November and December. The images revealed that the highest rate of enhancement occurred in April, with 5 out of the 8 images. January and July also show some images with enhancement (two out of three and two out of four, respectively). In March (three images), November (10 images) and December (six images), enhancement at Aldabra is unlikely.

Two other islands in the south-west Indian Ocean also generated an enhancement of

Table 1. *Frequency of biological enhancement in CZCS images. The columns headed E denote enhancement, PE possible enhancement. N no enhancement and T total*

	Aldabra				Cosmoledo				Iles Glorieuses Group			
Month	E	PE	N	T	E	PE	N	T	E	P	EN	T
January	1	1	1	3					2		1	3
February		1	1	2						1	1	2
March			3	3			3	3			3	3
April	3	2	3	8	3	1		4	3		4	7
May		1	1	2	1		1	2		1	1	2
June		1	2	3	1		2	3		1		1
July	2		2	4	1			1			4	4
August		1		1	1		1	2	1		1	2
September	1		1	2	1			1			1	1
October		1	1	2			1	1			1	1
November		3	7	10	4	1	1	6			9	9
December		3	3	6	3		1	4	1	1	4	6
Total	7	14	25	46	15	2	10	27	7	4	30	41

chlorophyll concentration at certain times. The atoll of Cosmoledo (47°40′ E, 9°30′ S) has a smaller proportion of enhancement occasions (showing increased chorophyll to the north-west in Fig. 4). Cosmoledo has approximately half the diameter of Aldabra and lies just upstream. The other region showing enhancement is near the Iles Glorieuses group (47°30′ E, 11°30′ S), similar in size to Cosmoledo. Here 15 images showed significant enhancement, and two showed a small effect, out of a total of 27 cloud-free images. The seasonal distribution is similar to that at Aldabra, except that images in November and December show a very high probability of enhancement, whereas Aldabra showed very little effect during this time. It is probable that this island group, lying further south in the main stream of the SEC, near Madagascar, is in a region of significantly stronger current than Aldabra.

4. THEORY

Aldabra presents an approximately elliptical profile to the incident flow (Fig. 1). Existing theory for rotating flow past obstacles is mainly for circular cylinders. We will take this to be applicable to our situation for the moment. Work by Page (1983) suggests that, for the contrasting model of Aldabra as a thin plate facing into the stream, separation of flow requires a greater ratio of non-linearity to viscosity (or Reynolds number) than for the circular cylinder theory to be discussed below.

For flow past a circular cylinder the presence or absence of a wake is determined by the importance of non-linearity in the flow compared to friction. In non-rotating flow the form of the wake is dictated by the Reynolds number (Batchelor, 1967)

$$R_e = \frac{2Ur}{A} \tag{1}$$

where U is the upstream speed, r the radius of the cylinder and A the horizontal eddy viscosity [10^2–10^5 m^2s^{-1} in the ocean (Apel, 1987), 10^2 m^2s^{-1} in the standard run of the numerical model of Section 6].

The boundaries between different flow regimes have been discussed by Batchelor (1967), Tritton (1977) and Kundu (1990), although no precise values are known. For low Reynolds number ($R_e < 1$) there is no wake, that is, there is no noticeable asymmetry between the flow on the upstream and downstream sides of the cylinder. This is referred to as fully attached flow. For a Reynolds number between 1 and about 40, trapped eddies occur downstream of the cylinder, while for Reynolds numbers greater than 40 the eddies are shed to form a vortex wake. As the Reynolds number increases from 40 to 80, instabilities form in the wake downstream of the cylinder and amplify to form a Karman vortex street, which decays downstream. For Reynolds numbers above 80, attached eddies are shed directly from the obstacle into the vortex street. For the A of the reduced gravity model to be discussed in the next section, the maximum Reynolds number is $O(100)$, suggesting that eddy shedding should be observed for strong currents.

The frequency, n, of eddies shed from an obstacle is usually described by the non-dimensional Strouhal number (Tritton, 1977)

$$S_t = \frac{2nr}{U}. \tag{2}$$

Here n is determined from a pair of eddies, that is, one cyclonic and one anticyclonic, or one from each side of an obstacle. The Strouhal number is a function of the Reynolds

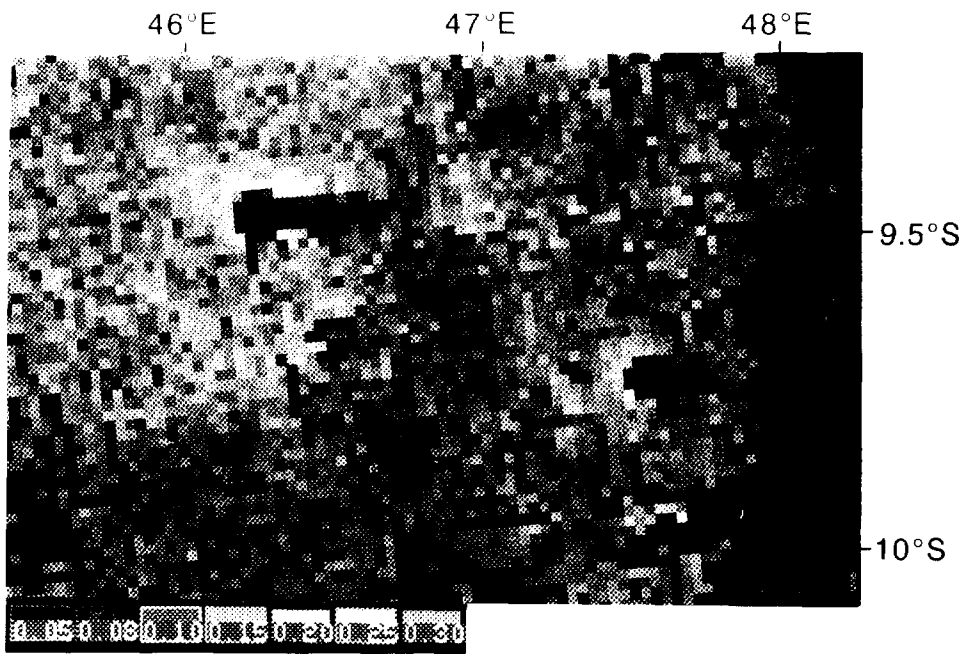

Fig. 4. A sample CZCS image of the southeast Indian Ocean taken on the 20 January 1983.

number. Birkhoff and Zarantonello (1957) and Roshko (1954) give empirical formulae valid for two-dimensional flow around a circular cylinder with $40 < R_e < 1000$. These show that the eddy shedding asymptotes to $S_t = 0.21$ with high R_e. The laboratory experiments of Boyer and Davies (1982) gave a value of 0.196 for S_t, while they quote 0.235 as the comparable parameter from the observations of atmospheric vortices by Chopra and Hubert (1965). For rectangular obstacles Ohya *et al.* (1992), using a numerical model, have shown that S_t suffers a series of discrete increases in shedding frequency as the length/width ratio increases. This is ascribed to a shear instability. Aldabra's length/width ratio does not approach their lowest experimental value for any realistic incident current.

Introducing rotation to the system adds several dynamical features (we will not consider the beta-effect, as Aldabra is too small for latitudinal change in the Coriolis parameter to be important; see Johnson and Page (1993) for how this affects the flow in the vicinity of an obstacle). Cyclonic eddies preferentially form in the wake of the cylinder. An additional, and often dominant, component of the momentum equation is the geostrophic relation. An indication of the relative importance of rotation is the Rossby number

$$R_o = \frac{U}{2\omega r}, \tag{3}$$

where ω is the rotation rate of the fluid. This is the ratio of the inertial and Coriolis terms in the momentum equation. Here it is $O(1)$. The Ekman number determines the size of any boundary wake; it is the ratio of frictional and Coriolis terms in the momentum equation, given by

$$E_k = \frac{A}{2\omega r^2}, \tag{4}$$

which is $O(10^{-2})$ for the standard runs of our reduced gravity model. Most theory for flow past a circular cylinder is only formally valid for small Rossby and Ekman number ($R_o, E_k < 1$); however, this is usually the case for the situations discussed here.

As seen earlier, the presence of a wake is related to the importance of the non-linear effects compared to friction. Walker and Stewartson (1972) showed that the existence of a wake required that

$$R_o > \frac{r}{H}\left(\frac{E_k}{2}\right)^{\frac{1}{2}}, \tag{5}$$

where H is the height of the cylinder. In our case, it is only the upper 150 m which flow past the island, so we take H to be 150 m. Since the radii, r, of the islands we discuss are some tens of kilometers, the right hand side of the inequality (5) becomes very large compared to R_o. This would imply that frictional forces are too strong to permit a wake.

The laboratory experiments of Baines and Davies (1980) and Boyer and Davies (1982) support the criterion (5) for non-attached flow. They derive regime boundaries as functions of R_o and E_k, which determine when trapped eddies or eddy shedding occur. These are discussed further in Section 7.2.

The theoretical work of Page (1985) discusses the regime boundaries for eddy formation, explaining the criterion of Walker and Stewartson (1972) in more detail. His flow is between two parallel plates with the Rossby and Ekman numbers defined in terms of the plate separation rather than the width of the cylindrical obstacle. As with laboratory experiments, he considers only the situation where the cylinder radius is similar to its height.

5. THE NUMERICAL MODEL

It is well known (Philander, 1990) that the dominant response of tropical oceans is from the first baroclinic mode. With this in mind a one-layer reduced gravity model is used for the numerical experiments. That is, we have an active upper layer overlying a deep quiescent ocean. The full nonlinear horizontal processes are retained. The model equations are

$$\frac{\partial u}{\partial t} + \Gamma(u) - fv = -\frac{g'}{a\cos\phi}\frac{\partial \eta}{\partial \lambda} + \frac{\tau^{\lambda}}{\rho\eta} + A\left(\nabla^2 u + \frac{(1-\tan^2\phi)u}{a^2} - \frac{2\sin\phi}{a^2\cos^2\phi}\frac{\partial v}{\partial \lambda}\right), \tag{6}$$

$$\frac{\partial v}{\partial t} + \Gamma(v) + fu = -\frac{g'}{a}\frac{\partial \eta}{\partial \phi} + \frac{\tau^{\phi}}{\rho\eta} + A\left(\nabla^2 v + \frac{(1-\tan^2\phi)v}{a^2} + \frac{2\sin\phi}{a^2\cos^2\phi}\frac{\partial u}{\partial \lambda}\right), \tag{7}$$

$$\frac{\partial \eta}{\partial t} + \Gamma(\eta) = 0, \tag{8}$$

where

$$\Gamma(\mu) = \frac{1}{a\cos\phi}\frac{\partial}{\partial \lambda}(u\mu) + \frac{1}{a\cos\phi}\frac{\partial}{\partial \phi}(v\mu\cos\phi),$$

$$\nabla^2(\mu) = \frac{1}{a^2\cos^2\phi}\frac{\partial^2 \mu}{\partial \lambda^2} + \frac{1}{a^2\cos\phi}\frac{\partial}{\partial \phi}\left(\frac{\partial \mu}{\partial \phi}\cos\phi\right).$$

The variables λ, ϕ, u, v, η, τ^{λ}, τ^{ϕ} represent longitude, latitude, zonal velocity, meridional velocity, layer thickness, zonal wind stress and meridional wind stress, respectively. The radius of the Earth is a, and f is the constant Coriolis parameter. The density of the active upper layer is ρ and the coefficient for horizontal eddy viscosity is A. The reduced gravity is $g' = g\Delta\rho/\rho$, where $\Delta\rho$ is the density difference between the upper and lower layers. No slip boundary conditions are used on all lateral boundaries.

The model is discretized in the horizontal using an Arakawa "B" type grid. The finite difference scheme, which is based on the horizontal component of the scheme of Cox (1984), uses centred differencing in space and leapfrogging in time. This results in three explicit prognostic equations for u, v and η, which can be simply stepped forward in time. A Robert time filter, as described by Asselin (1972), is used to remove the computational mode associated with leapfrogging.

6. THE NUMERICAL EXPERIMENTS

The model is configured as a periodic channel (to avoid the complication of open boundary conditions) in which islands of arbitrary shape and size can be placed. For the experiments described below, the shape of the island of Aldabra (taken from the 1000 m isobath) is placed in the channel as if it were facing a westward current or a northward current (see Fig. 2). The horizontal extent of the channel is 550 km by 280 km, and the horizontal resolution is 2.7 km. The reduced gravity g' has the value 2.94×10^{-2} m s^{-1}. The ocean is initially at rest with the thickness of the upper layer set to 150 m. The model is integrated forward with timesteps of 7.5 min. For most of the experiments discussed in

Section 7 the constant eddy viscosity A takes the value 10^2 m^2 s^{-1}. Section 7.4 examines the effect of varying this parameter.

Two techniques were used to produce a representation of the SEC. Initial experiments used a westward wind stress at the ocean surface to accelerate the current to a predetermined value, after which the wind stress was switched off. As there is little friction in the model, the current decays in strength very slowly. In this case eddies would readily form behind the island and be swept downstream. This occurred even for lower Reynolds numbers than predicted by theory. The reason appeared to be the cyclic nature of the model. Disturbances to the upstream flow, however small, appeared to enhance the eddy shedding process. This approach, while being noted, was abandoned because the random nature of the disturbances to the upstream flow made comparisons with theory difficult. However, it should be remembered that in the real ocean upstream flows are unlikely to be uniform, and so eddy shedding may be more ubiquitous than our more formal experiments suggest.

A second approach, which was used for the majority of our numerical experiments, was to use a westward wind stress to drive a purely zonal flow in the channel without any obstruction. The flow field and corresponding interface thickness were saved for various flow rates in the centre of the channel. The model was then configured with a forcing/damping region in which the velocity field and layer thickness were relaxed to values for a certain flow rate. This had the combined effect of producing a constant upstream flow and preventing any disturbances from propagating around the channel. The model could then be run for any desired upstream flow rate and island shape. For the results described below upstream currents of up to 1 m s^{-1} were considered. Stronger flows result in numerical instability in the presence of an obstruction to the flow.

A number of additional experiments were performed with a circular island of radius 18 km. These experiments allowed for a greater exploration of parameter space, and in particular the effect of rotation and different coefficients of eddy viscosity.

7. RESULTS

7.1. *Flow patterns*

At low Reynolds numbers (and incident speeds) the flow is not much disturbed by the presence of the island, and no eddies form in the lee of the island. Such a situation is illustrated in Fig. 5 for the case of an incident flow of 0.05 m s^{-1} from the east ($R_e = 11$). There is a wake, indicated by weaker current vectors, extending a number of island lengths downstream. For higher Reynolds numbers (and incident speeds) trapped eddies appear immediately behind the island. An example is shown in Fig. 6 for the case of an incident flow of 0.1 m s^{-1} from the south ($R_e = 47$). The eddies are apparent in both the active upper layer thickness (a proxy for streamlines) and in the current vectors. The flow field looks qualitatively similar to that produced by Falconer *et al.* (1986) for shallow water tidal-driven flow past Rattray island (dimensions 1.5 km by 300 m). As Reynolds numbers (and incident speeds) are increased further, the model produces instabilities in the wake. Finally at even higher Reynolds numbers the model successfully predicts a wake of shed eddies, a Karman vortex street. Figure 7 illustrates the response of the model when the island is impacted by an incident speed of 0.8 m s^{-1} from the east ($R_e = 178$). The time-averaged state (Fig. 7(a)) shows little disturbance to flow after just two island lengths downstream. An instantaneous picture (Fig. 7(b)) shows an anticyclonic eddy forming at the southern edge of

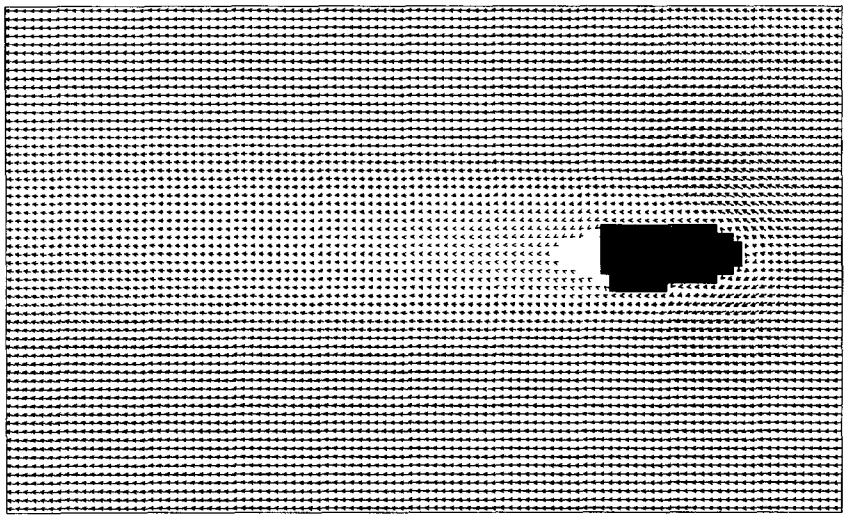

Fig. 5. The model steady state response at low Reynolds number (11) with flow from the east, illustrated by velocity vectors in the active upper layer. The distance between grid points is equivalent to 0.05 m s^{-1}.

the island's lee. Other eddies of alternating direction can be seen propagating downstream. These features are more clearly illustrated (Fig. 7(c)) in the anomaly field (instantaneous–mean). These patterns are similar to those observed in laboratory experiments (Boyer and Kmetz, 1983).

Figure 8 illustrates the eddy formation process in terms of shedding of relative vorticity for incident flow from the east. For speeds up to 0.4 m s^{-1} ($R_e = 89$), vorticity of opposite sign is shed from each side of the island and swept smoothly and steadily downstream. As the incident velocity is increased (0.45 m s^{-1}, $R_e = 100$), a transition takes place and transient meanders appear in the vorticity that are swept downstream. At even greater incident velocities (0.8 m s^{-1}, $R_e = 178$), the wake becomes unstable and isolated patches of vorticity are shed downstream.

7.2. *Thresholds for eddy shedding into a vortex street*

When the island presents its narrowest cross-section to the flow (incident flow from the east—the "thin island" case, Table 2), eddies are shed periodically for incident speeds of 0.45 m s^{-1} and above. When the flow is from the south, the island presents its widest cross-section (the "thick island" case, Table 3), and eddies begin to be shed at lower speeds: 0.15 m s^{-1}. This result is expected since eddies are shed for larger Reynolds numbers and R_e increases linearly with the length scale blocking the flow. We note that, since Aldabra is approximately twice as long east–west as it is north–south, flows from the east would have to be twice as fast as flows from the south to have the same influence on the biological community, through eddy formation and shedding.

In our model, for $R_e < 40$, no eddies are apparent. For slightly larger R_e, eddies do appear downstream, but when the model is run for many days the eddies decay; the equilibrium

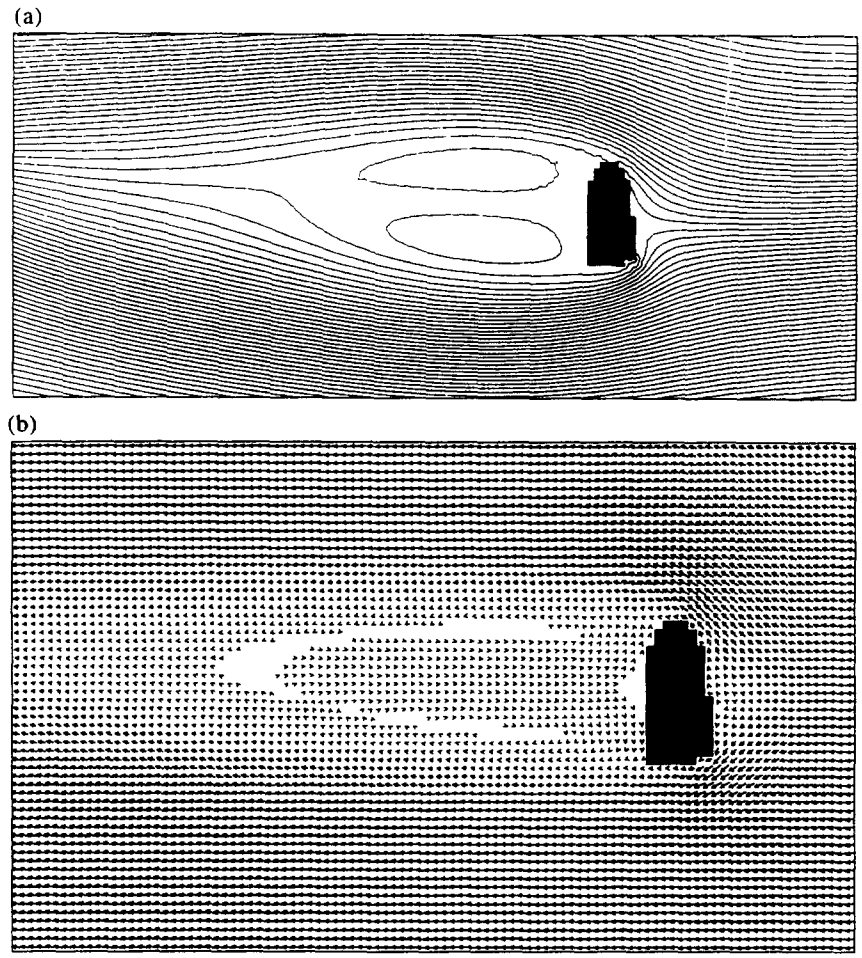

Fig. 6. The model steady state response at medium Reynolds number (47) with flow from the south. (a) Contours of upper layer depth. The contour interval is 0.1 m. (b) Velocity vectors in the upper layer. The distance between grid points is equivalent to 0.1 m s^{-1}.

situation is reached after a few months in which no eddies are shed. These eddies are a Karman vortex street derived from an instability of the wake, in accordance with theory and observations (Chopra and Hubert, 1965; Barkley, 1972). As R_e increases again, the eddies do not decay and are shed from directly behind the island. Eddies are shed at a threshold R_e of 100 for the thin island case, 71 for the thick island and 72 for the circular island. Clearly the more streamlined shape, as expected, is less inclined to shed eddies.

For a rotating flow, both Rossby and Ekman numbers determine the eddy shedding. Note that the Reynolds number is simply proportional to the ratio of the Rossby number to the Ekman number, so is not an independent parameter (Baines and Davies (1980) and Boyer and Kmetz (1983) define their Reynolds number as this ratio, so their R_e is half of ours). In Fig. 9 we compare our results with the flow scenarios found by Baines and Davies (1980) from laboratory experiments. Our Ekman numbers are greater than theirs, but it is clear

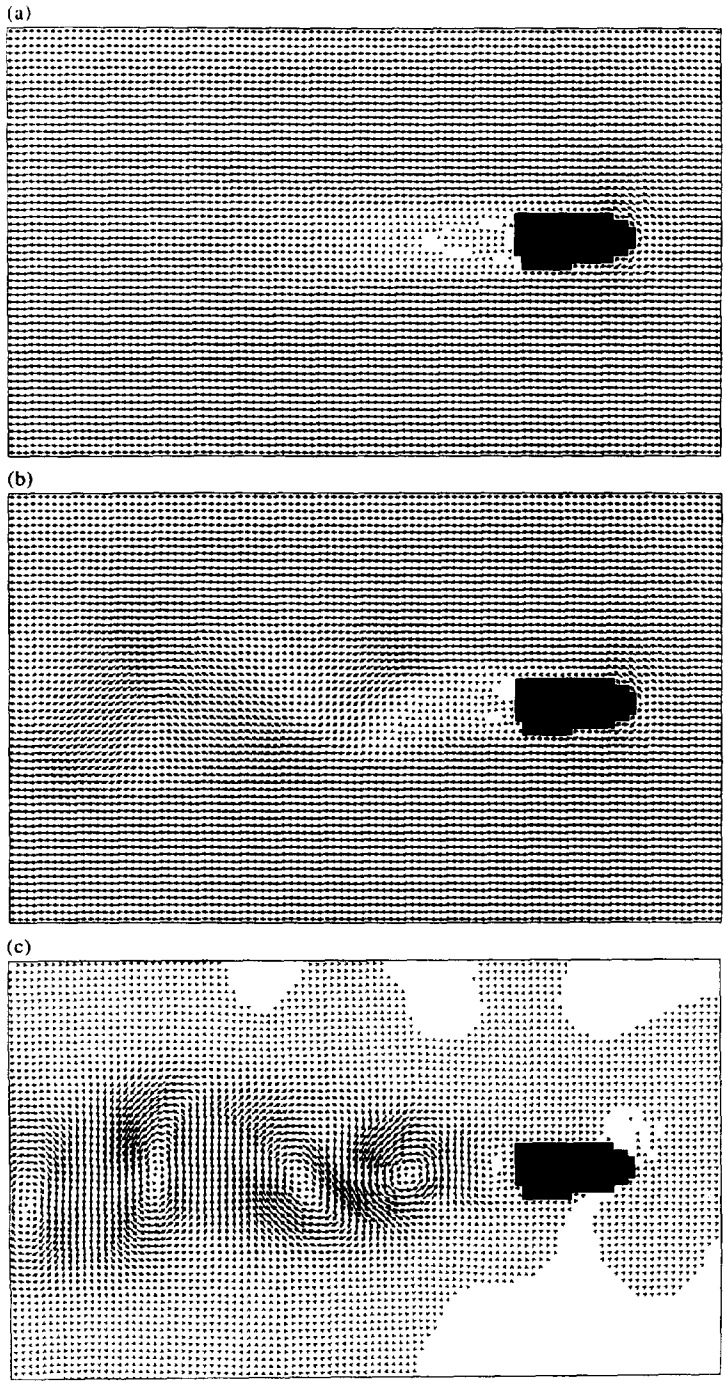
(a)
(b)
(c)

that eddies form and are shed in our model at much lower Rossby numbers than their figure shows. Our eddies are more in accordance with the traditional non-rotating theory using R_e as a threshold parameter. The condition of Walker and Stewartson (1972) also does not appear to be applicable since our values of R_o are always at least an order of magnitude smaller than $\frac{r}{H}(\frac{E_k}{2})^{\frac{1}{2}}$, yet eddies are shed in a large number of cases. The only obvious difference between the laboratory experiments of Boyer and Davies (1982) and our numerical experiments is the difference in aspect ratio of the cylinder. We believe our numerical experiments to be more relevant to the oceanic situation.

7.3. *Effect of rotation*

As was shown in laboratory experiments by Boyer and colleagues (Boyer and Davies, 1982; Boyer and Kmetz, 1983; Boyer *et al.*, 1984), the effect of rotation is to enhance the cyclonic eddies at the expense of the anticyclonic ones. Even at 10°S, we confirm that this effect occurs in the ocean to some extent. Rotation also affects the regime boundaries, as is shown in Fig. 9. We have already seen that at the latitude of Aldabra the numerical results are in closer agreement with non-rotating flow (that is, using R_e thresholds rather than those of Baines and Davies (1980)). In Table 4 and Fig. 10 we show the impact of 3 different f-values, corresponding to 20°S and 30°S as well as Aldabra (9°45′ S) for a circular island. Stronger rotation (that is smaller Ekman numbers) alters the regime bands, pushing their slope towards those of the laboratory experiments, although the transitions remain at much lower R_o than these suggest. That is, increasing the rotation rate tends to inhibit the shedding of eddies. For computational stability reasons we are unable to run the model at higher latitudes, but one might speculate that at higher rotation rates the thresholds for eddy shedding might be more in accordance with those of Baines and Davies (1980).

7.4. *Effect of eddy viscosity*

The effect of the model eddy viscosity was examined by running the model with a number of values ($A = 10^2$, 2×10^2, 3×10^2, 5×10^2, 10^3 m^2 s^{-1}) for the circular island case with an incident velocity of 0.5 m s^{-1}. The results are shown in Table 4 and illustrated on the regime diagram (Fig. 10). Increasing the eddy viscosity increases the Ekman number, decreases the Reynolds number, and, as one would expect, tends to have a stabilizing effect on the flow. With the standard value of $A = 10^2$ m^2 s^{-1} a Karman vortex street is shed downstream. This is also the case for $A = 2 \times 10^2$ m^2 s^{-1}. For $A = 3 \times 10^2$ m^2 s^{-1}, eddy shedding occurs during the spin-up process, but eventually decays. For $A > 5 \times 10^2$ m^2 s^{-1} no eddies are formed. These results are consistent with the Reynolds number thresholds of the standard run.

7.5. *Periodicity of eddy shedding*

We have determined the Strouhal number by counting (from figures such as Fig. 11) the eddy pairs shed from the island into the wake, once equilibrium has been reached. These are

Fig. 7. The model response at high Reynolds number (178) with flow from the east. (a) Time mean velocity vectors in the upper layer. The distance between grid points is equivalent to 0.8 m s^{-1}. (b) Instantaneous velocity vectors in the upper layer. The distance between grid points is equivalent to 0.8 m s^{-1}. (c) Instantaneous-time mean velocity vectors in the upper layer. The distance between grid points is equivalent to 0.2 m s^{-1}.

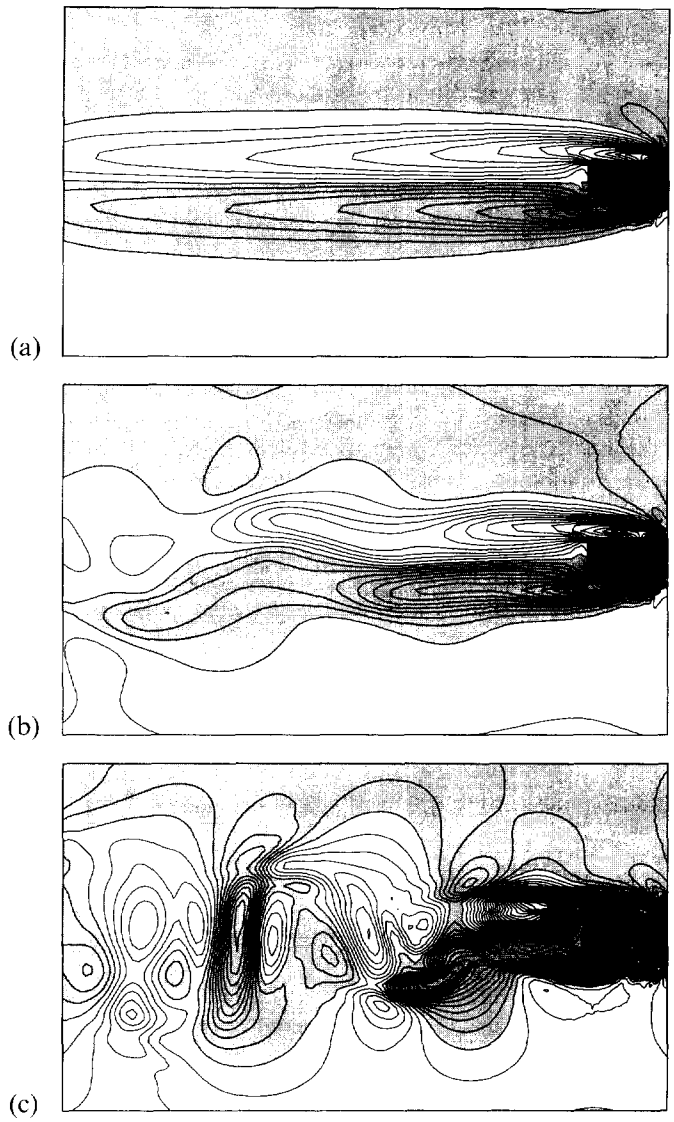

Fig. 8. Instantaneous contours of relative vorticity for incident velocities of (a) 0.4 m s^{-1}, (b) 0.45 m s^{-1} and (c) 0.8 m s^{-1}. The contour interval is 2×10^{-6} s^{-1} and regions of negative vorticity are shaded.

plotted as a function of Reynolds number in Fig. 12. The non-rotating empirical relationships of Roshko (1954) and Birkhoff and Zarantonello (1957) are similar, so only that of Birkhoff and Zarantonello is plotted on Fig. 12. Boyer and Kmetz (1983) have undertaken laboratory experiments to determine the effect of rotation on Strouhal number, again for a cylinder (but with $r \sim d$). They also investigate the effect of aspect ratio (height/radius). Their results showed Strouhal numbers greater than those predicted for the non-rotating case, particularly at Reynolds numbers around 400 (they have few cases for the

Table 2. The incident speed and non-dimensional parameters for flow from the east of Aldabra (across stream radius 11.1 km, *along stream radius* 23.6 km). *The Ekman number is* 0.032 *and the value of* $\frac{r}{H}(\frac{E_k}{2})^{\frac{1}{2}}$ *is* 9.4

U (m s^{-1})	R_e	S_t	R_o
0.05	11	—	0.18
0.10	22	—	0.36
0.15	33	—	0.54
0.20	44	—	0.72
0.25	56	0.262*	0.90
0.30	67	0.273*	1.08
0.35	78	0.281*	1.26
0.40	89	0.273*	1.44
0.45	100	0.283	1.62
0.50	111	0.300	1.80
0.60	133	0.330	2.16
0.80	178	0.350	2.89
1.00	222	0.355	3.61

*Indicates that eddy shedding eventually decays.

lower Reynolds numbers we are concerned with in the ocean). Our results show that the thin island case (westward flow) exhibits lower Strouhal numbers than the relationship given above, while the thick island (northward flow) shows higher Strouhal numbers. Both cases follow similar curves; the Strouhal number appears constant for $40 < R_e < 70$ (the Karman vortex shedding regime), increases rapidly for Reynolds numbers between 70 and 150 (once discrete eddy shedding begins), and increases very little thereafter. The curve for a circular island always lies between the two, but has a lower asymptote than experiments suggest.

Table 3. The incident speed and non-dimensional parameters for flow from the south of Aldabra (across stream radius 23.6 km, *along stream radius* 11.1 km). *The Ekman number is* 0.007 *and the value of* $\frac{r}{H}(\frac{E_k}{2})^{\frac{1}{2}}$ *is* 9.4

U (m s^{-1})	R_e	S_t	R_o
0.10	47	0.071*	0.167
0.15	71	0.062	0.250
0.20	95	0.071	0.334
0.25	119	0.082	0.417
0.30	142	0.091	0.501
0.35	166	0.096	0.584
0.40	190	0.095	0.668
0.45	213	0.097	0.751
0.50	236	0.099	0.834
0.70	330	0.094	1.168
0.75	354	0.085	1.252
0.80	377	0.082	1.335

*Indicates that eddy shedding eventually decays.

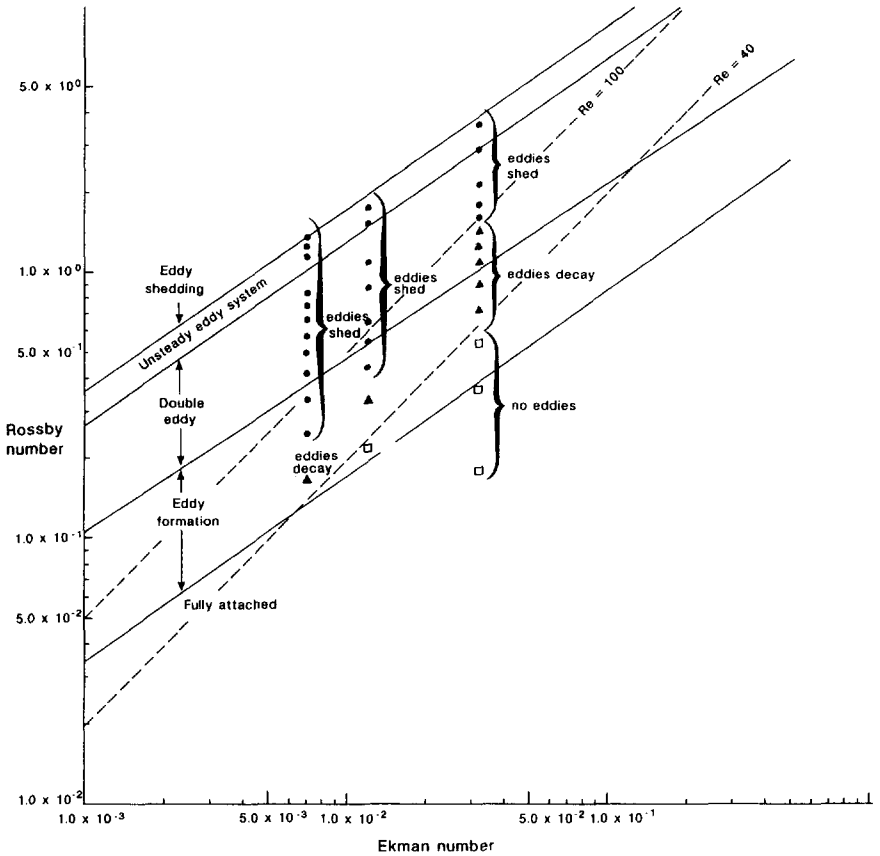

Fig. 9. Rossby number/Ekman number flow regime diagram showing the regime boundaries from Baines and Davies (1980) (solid lines) and Reynolds numbers of 40 and 100 (dashed lines). Results are shown for three different island scenarios at 9°45'S, see Tables 2–4.

The thin island case sheds fewer eddies, for a given Reynolds number, than the circular or thick island cases. Note that numerical stability problems at the highest Reynolds numbers tend to lower the fast flow Strouhal numbers below the asymptotes (Fig. 12).

7.6. *Downstream eddy speed*

Theory for an infinite cylinder in a non-rotating flow (Chopra and Hubert, 1965) predicts that the translation speed of the eddies downstream U_e should be 85% of the incident speed U regardless of distance downstream. Boyer and Kmetz (1983) measured U_e/U in laboratory experiments. They explain that eddy suction causes their eddies to decay rapidly, and under these circumstances the ratio U_e/U tends to 1 at distances downstream greater than 10 island radii. Our eddy speed is determined slightly earlier than this; unlike those observed in the laboratory experiments, our eddies appear to travel more quickly immediately after leaving the island, and then to settle into a downstream speed of about 85% of U. Our results indicate that the ratio is slightly smaller at lower R_e ($R_e < 100$).

Table 4. The incident speed, eddy viscosity, equivalent latitude of Coriolis parameter and non-dimensional parameters for flow past a circular island radius 18 km

U (m s^{-1})	A (m^2 s^{-1})	Latitude of f	R_e	S_t	R_o	E_k	$\frac{r}{H}(\frac{E_k}{2})^{\frac{1}{2}}$
0.10	10^2	9°45′S	36	—	0.219	0.0122	9.4
0.15	10^2	9°45′S	54	—	0.328	0.0122	9.4
0.20	10^2	9°45′S	72	0.132	0.437	0.0122	9.4
0.25	10^2	9°45′S	90	0.147	0.547	0.0122	9.4
0.30	10^2	9°45′S	108	0.160	0.656	0.0122	9.4
0.40	10^2	9°45′S	144	0.164	0.875	0.0122	9.4
0.50	10^2	9°45′S	180	0.175	1.084	0.0122	9.4
0.50	2×10^2	9°45′S	90	0.145	1.084	0.0244	13.3
0.50	3×10^2	9°45′S	60	0.129*	1.084	0.0366	16.2
0.50	5×10^2	9°45′S	36	—	1.084	0.061	21.0
0.50	10^3	9°45′S	18	—	1.084	0.122	29.6
0.70	10^2	9°45′S	252	0.179	1.537	0.0122	9.4
0.80	10^2	9°45′S	288	0.177	1.757	0.0122	9.4
0.20	10^2	20°S	72	0.125*	0.223	0.0062	6.7
0.30	10^2	20°S	108	0.130	0.335	0.0062	6.7
0.50	10^2	20°S	180	0.113	0.558	0.0062	6.7
0.20	10^2	30°S	72	—	0.151	0.0042	5.5
0.50	10^2	30°S	180	0.089*	0.381	0.0042	5.5

*Indicates that eddy shedding eventually decays.

7.7. *Dynamic uplift*

From the point of view of the biological significance of flow disturbance by islands, it has been suggested that it is the thinning of the upper layer downstream that is important (Heywood *et al.*, 1990). If the thermocline is raised ("dynamic uplift"), nutrients are brought within the photic zone, and primary productivity may be enhanced. This is indeed what happens in our model (Fig. 13). Upstream of the island, the thermocline is depressed. Downstream, the thermocline is raised, but not to the extent observed (~ 10 m rather than ~ 30 m). This is almost certainly due to the vertically averaged nature of the dynamics in the active upper layer of the model.

8. CONCLUSIONS

Using a reduced physics model we have examined the parameter regime for shedding of eddies from oceanic islands. In particular we have focused on the tropical island of Aldabra. Unlike observational studies of the real ocean, we are able to prescribe eddy viscosity and incident flow speeds to establish circumstances for eddy formation and shedding. In summary, increasing the viscosity and rotation rate reduce the likelihood of eddy formation, whilst increasing the speed of incident flow and the width of the island increase the likelihood of eddy formation. Our numerical results show that, for the parameter regime to be expected for low-latitude islands in the ocean, non-rotating theory using R_e as a threshold parameter is appropriate. Transitions from no flow to attached eddies, to shedding discrete long-lived eddies occur at significantly lower R_o than the rotating laboratory experiments of Boyer and Davies (1982). At higher latitudes, and thus stronger rotation, the transition

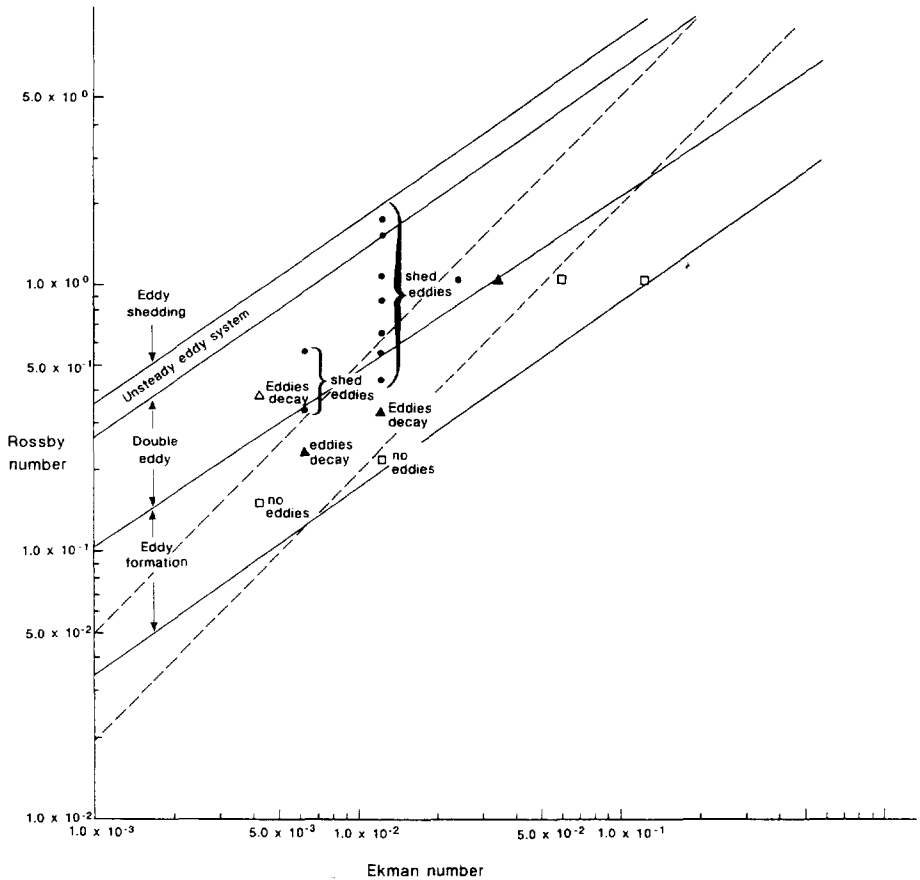

Fig. 10. Rossby number/Ekman number flow regime diagram showing the regime boundaries from Baines and Davies (1980) (solid lines) and Reynolds numbers of 40 and 100 (dashed lines). Results are shown for a circular island at different latitudes and different eddy viscosities, see Table 4.

regimes are shifted toward higher R_o. Most laboratory studies suggest rotation to be important, but their parameter regimes are usually more applicable to the atmosphere than the ocean, and it is possible that differences between these studies and ours are due to a different height-to-width ratio of the obstacle. Observations have previously noted this weak dependence on rotation (Pattiaratchi *et al.*, 1986) and that R_e is a good measure of flow regime (Barkley, 1972; Tomczak, 1988).

The numerical model is able to confirm many of the phenomena seen in laboratory experiments or predicted theoretically (for example, the speed of eddies advected downstream behind the island). Most laboratory experiments are undertaken with circular cylinders. We have used a real island shape (although with vertical sides) and considered the differences between incident flow from two different directions. As would intuitively be expected, the more streamlined island begins to shed eddies at a higher Reynolds number threshold, and sheds eddies less frequently for a given R_e. The Strouhal numbers of the

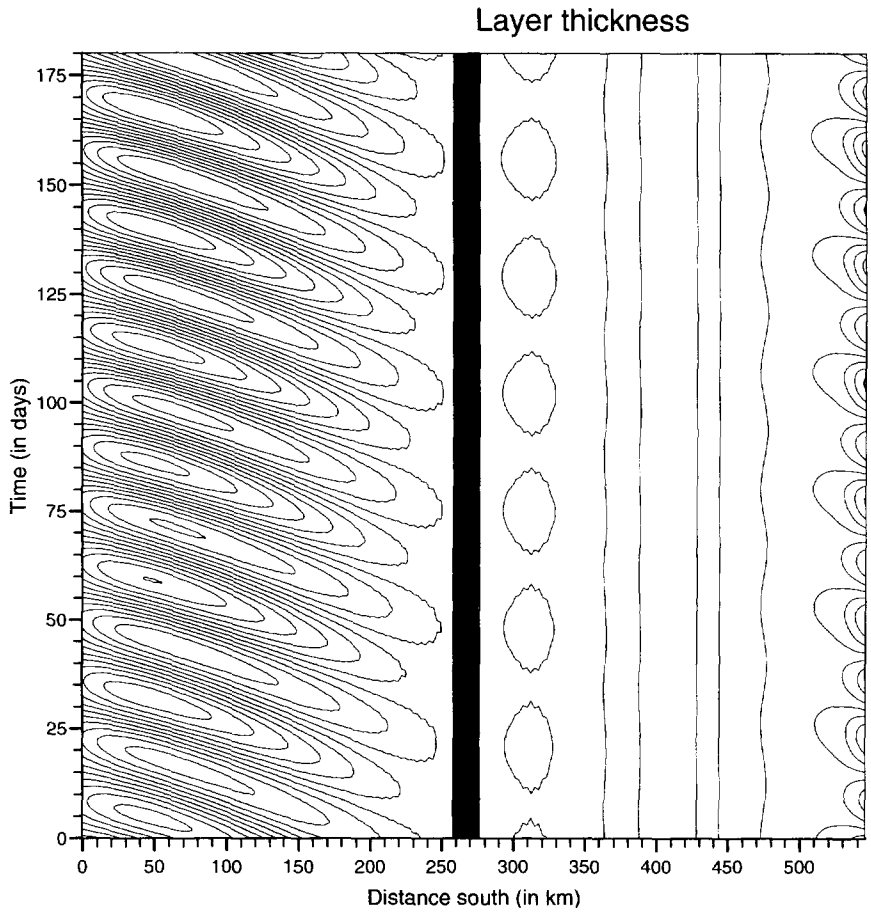

Fig. 11. The thickness of the active upper layer as a function of time and distance southward for the flow past Aldabra from the south at an incident speed of 15 cm s^{-1}. The contour interval is 0.25 m. The forcing/damping region, south of the island, is clearly visible.

numerical model are in agreement with theoretical predictions, all shapes leading to a stable Strouhal number as R_e increases.

This study suggests that the generation of island wake eddies should occur at lower flow speeds than laboratory experiments (Boyer and Davies, 1982) and some theories (Page, 1985) suggest. The climatological flow fields for Aldabra together with the model results suggest that eddy shedding should be common from May to October. Many of the surface currents of the world oceans have flows in excess of the 0.15–0.25 m s^{-1} required for eddy generation from islands of this size. Enhanced biological productivity due to eddy formation may be a common phenomenon in some regions, and potentially a significant factor in the global exchange of CO_2 between atmosphere and ocean. Our initial experiments, where eddy generation was initiated for even lower R_e in an unsteady incident flow, carry the implication that such a contribution to the global carbon budget may be even more significant.

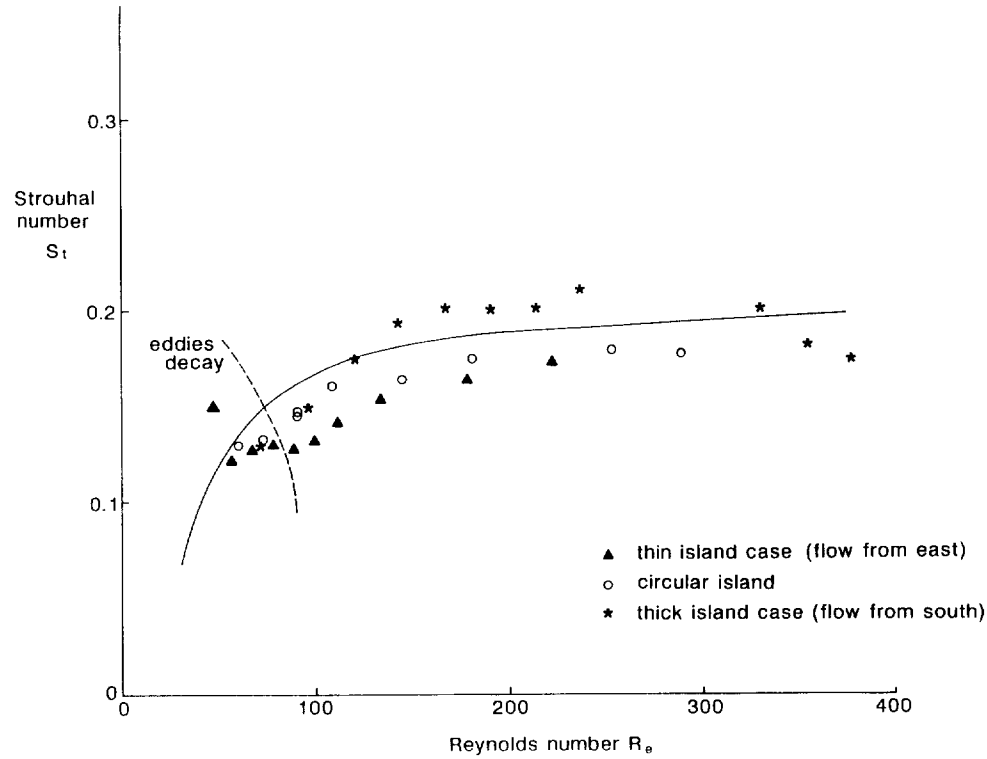

Fig. 12. A plot of Strouhal number against Reynolds number. The solid line represents the non-rotating empirical relationship of Birkhoff and Zarantonello (1957), the triangle represents the case of Aldabra with flow from the east, the asterisk represents the case of Aldabra with flow from the south, and the circle represents the case of the circular island.

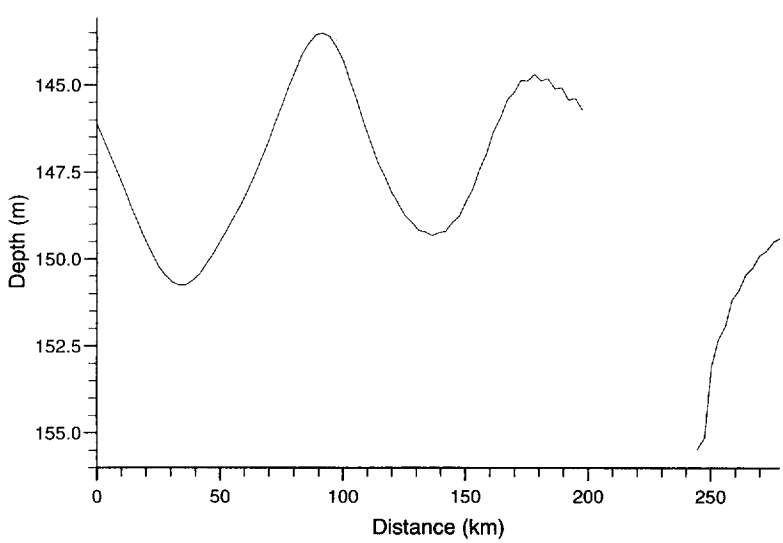

Fig. 13. The thickness of the active upper layer on an east–west section passing through the island. The incident current is 0.6 m s^{-1} from the east.

Acknowledgements—The CZCS images were kindly supplied by Jeff Whiting at GSFC, NASA. The authors are most grateful to Des Barton (School of Ocean Sciences, University of Wales, Bangor) for permission to use Fig. 2, results from his cruise 24 on R.R.S. *Charles Darwin*. The helpful comments of two anonymous referees are also gratefully acknowledged.

REFERENCES

Anderson D. L. T. and D. J. Carrington (1993) Modelling interannual variability in the Indian Ocean using momentum fluxes from the operational weather analyses of the United Kingdom Meteorological Office and European Centre for Medium Range Weather Forecasts. *Journal of Geophysical Research*, **98**, 12,483–12,499.

Apel J. R. (1987) *Principles of ocean physics*, Academic Press, Orlando, FL, U.S.A., 631 pp.

Asselin R. (1972) Frequency Filter for time integrations. *Monthly Weather Review*, **100**, 487–490.

Baines P. G. and P. A. Davies (1980) Laboratory studies of topographic effects in rotating and/or stratified fluids. In: *Orographic effects in planetary flows*, R. Hide and P. White, editors. GARP Publ. Ser., 23, WMO, Geneva, 233–299.

Barkley R. A. (1972) Johnston Atoll's Wake. *Journal of Marine Research*, **30**, 201–216.

Batchelor G. K. (1967) *An introduction to fluid dynamics*. Cambridge University Press, Cambridge, U.K., 515 pp.

Birkhoff G. and E. H. Zarantonello (1957) *Jets, wakes and cavities*. Academic Press, Orlando, FL, U.S.A., 353 pp.

Boyer D. L. and P. A. Davies (1982) Flow past a circular cylinder on a β-plane. *Philosophical Transactions of the Royal Society of London, Series A*, **306**, 533–556.

Boyer D. L. and M. L. Kmetz (1983) Vortex shedding in rotating flows. *Geophysical and Astrophysical Fluid Dynamics*, **26**, 51–83.

Boyer D. L., M. L. Kmetz, L. Smathers, G. Charbert d'Hieres and H. Didelle (1984) Rotating open channel flow past right circular cylinders. *Geophysical and Astrophysical Fluid Dynamics*, **30**, 271–304.

Chopra K. P. and L. F. Hubert (1965) Mesoscale eddies in the wake of islands. *Journal of the Atmospheric Sciences*, **22**, 652–657.

Cox M. D. (1984) A Primitive Equation, 3-Dimensional Model of the Ocean. GFDL Ocean Group Tech. Rep. No. 1, University of Princeton, NJ.

Cutler A. N. and J. C. Swallow (1984) Surface Currents of the Indian Ocean (to 25°S, 100°E). Report 187, Institute of Oceanographic Science, Wormley, Surrey, U.K., 8 pp.

Falconer R. A., E. Wolanski and L. Mardapitta-Hadjipandeli (1986) Modeling Tidal Circulation in an Island's Wake. *Journal of Water Port, Coastal Ocean Engineering*, **112**, 234–254.

Gilmartin M. and N. Revelante (1974) The "island mass" effect on the phytoplankton and primary production of the Hawaiian islands. *Journal of Experimental Marine Biology and Ecology*, **16**, 181–204.

Gjevik B. (1980) Orographic effects revealed by satellite pictures: mesoscale flow phenomena. In: *Orographic effects in planetary flows*, R. Hide and P. White, editors. GARP Publ. Ser., 23, WMO, Geneva, pp. 301–316.

Heywood K. J., E. D. Barton and J. H. Simpson (1990) The effects of flow disturbance by an oceanic island. *Journal of Marine Research*, **48**, 55–73.

Heywood K. J., S. Scrope-Howe and E. D. Barton (1991) Estimation of zooplankton abundance from shipborne ADCP backscatter. *Deep-Sea Research*, **38**, 677–691.

Hogg N. G. (1980) Effects of bottom topography on ocean currents. In: *Orographic effects in planetary flows*, R. Hide and P. White, editors. GARP Publ. Ser., 23, WMO, Geneva, pp. 167–205.

Johnson E. R. and M. A. Page (1993) Flow past a circular cylinder on a β-plane. *Journal of Fluid Mechanics*, **257**, 603–626.

Kundu P.K. (1990) *Fluid Dynamics*, Academic Press, Orlando, FL, U.S.A.

Ohya Y., Y. Nakamuva, S. Ozono, H. Tsuruta and R. Nakayama (1992) A numerical study of vortex shedding from flat plates with square and trailing leading edges. *Journal of Fluid Mechanics*, **236**, 445–460.

Page M. A. (1983) The low Rossby number flow of a rotating fluid past a flat plate. *Journal of Engineering Mathematics*, **17**, 191–202.

Page M. A. (1985) On the low Rossby number flow of a rotating fluid past a circular cylinder. *Journal of Fluid Mechanics*, **156**, 205–221.

Pattiaratchi C., A. James and M. Collins (1986) Island wakes and headland eddies: a comparison between remotely sensed data and laboratory experiments. *Journal of Geophysical Research*, **92**, 783–794.

Philander S. G. (1990) *El Nino, La Nina, and the Southern Oscillation*. Academic press, Orlando, FL, U.S.A., 293 pp.

Roshko A. (1954) *On the development of turbulent wakes from vortex streets*, N. A. C. A. Rep. 1191.

Scorer R. S. (1986) *Cloud investigation by satellite*. Ellis Harwood, Chichester, U.K.

Tomczak M. (1988) Island wakes in deep and shallow waters. *Journal of Geophysical Research*, **93,** 5153–5154.

Tritton D. J. (1977) *Physical fluid dynamics*, Van Nostrand Reinhold, New York, 362 pp.

Walker J. B. A. and K. Stewartson (1972) The flow past a circular cylinder in a rotating frame. *Zeitschrift fur Angewandte Mathematik und Physik*, **23,** 745–752.